Rapid Communications

Laser-driven plasma pinching in e^-e^+ cascade

E. S. Efimenko,[1] A. V. Bashinov,[1] A. A. Gonoskov,[1,2] S. I. Bastrakov,[3,2] A. A. Muraviev,[1]
I. B. Meyerov,[2] A. V. Kim,[1] and A. M. Sergeev[1]

[1]*Institute of Applied Physics, Russian Academy of Sciences, 603950 Nizhny Novgorod, Russia*
[2]*Lobachevsky State University of Nizhni Novgorod, 603950 Nizhny Novgorod, Russia*
[3]*Helmholtz-Zentrum Dresden-Rossendorf, 01328 Dresden, Germany*

(Received 31 August 2018; published 13 March 2019)

The cascaded production and dynamics of electron-positron plasma in ultimately focused laser fields of extreme intensity are studied by three-dimensional particle-in-cell simulations with the account of the relevant processes of quantum electrodynamics (QED). We show that, if the laser facility provides a total power above 20 PW, it is possible to trigger not only a QED cascade but also pinching in the produced electron-positron plasma. The plasma self-compression in this case leads to an abrupt rise of the peak density and magnetic (electric) field up to at least 10^{28} cm^{-3} and 1/20 (1/40) of the Schwinger field, respectively. Determining the actual limits and physics of this process might require quantum treatment beyond the used standard semiclassical approach. The proposed setup can thus provide extreme conditions for probing and exploring fundamental physics of the matter and vacuum.

DOI: 10.1103/PhysRevE.99.031201

In recent years there has been an increasing interest in the problem of electron-positron-pair plasma production by laser fields of extreme intensities. This problem could shed light on the long-standing questions related to extreme astrophysical events, such as jets and gamma-ray bursts [1]. The problem itself represents a great challenge in contemporary physics in the context of producing very dense pair plasmas in the laboratory [2]. A pioneering step was made by Bell and Kirk who showed that prolific pair generation can occur in a standing circularly polarized wave with an intensity of about 10^{24} W/cm^2 [3]. The subsequent investigations of laser fields of various configurations confirmed the possibility of efficient generation of electron-positron pairs and optimized field configurations were proposed [4–6]. The next important step was to use two-dimensional (2D) and three-dimensional (3D) simulations, mostly based on particle-in-cell (PIC) codes extended with probabilistic routines for the processes of quantum electrodynamics (QED). The simulations showed that dense pair plasma can be actually produced by tightly focused laser beams [7–9]. Furthermore, effective γ-ray sources in the GeV energy range were also proposed [10]. Estimates show that the forthcoming 10-PW-class laser facilities, such as the Extreme Light Infrastructure Facility [11], the Vulcan 10 PW upgrade [12], or Apollon 10 PW [13] are able to ignite the electron-positron cascade in vacuum. It was recently demonstrated that extreme states of pair plasmas in terms of densities, currents, and electric and magnetic fields can be produced in an optimally configured multibeam laser setup [14]. It should be also mentioned that along with this research a lot of fundamental issues of extremely intense laser field interactions with matter were raised and resolved, such as the processes of strong-field QED [15,16], the signatures of radiation reaction forces and radiation trapping effects in single-particle motion [6,17–21], and the nonlinear regimes of laser plasma interactions [14,22,23]. However, many of the fundamental features, especially related to nonlinear interactions of electron-positron plasmas with laser fields of extreme intensities, are still to be studied. This is especially true in the light of the next-generation projects, such as the XCELS [24], the Gekko-EXA [25], and the SEL [26], that are aimed at constructing multi-10-PW laser systems with power of up to 100 PW.

In this Rapid Communication we consider the cascaded production and the consequent self-action of electron-positron plasma spatially confined in a λ^3 volume initiated by the optimally focused laser radiation with a total power of multi-10-PW level. Here we assume that either some microscopic target or externally injected particles or photons seed the cascaded production of photons and electron-positron pairs. The cascade and the resulting electron-positron plasma are driven by the strong electromagnetic field, which is achieved at the intersection of several tightly focused laser beams forming the inverse emission of a dipole antenna (see Fig. 1 of the Supplemental Material [27]). We have revealed a fundamental feature of the field-driven electron-positron plasma, when an axial column of plasma current and self-generated azimuthal magnetic field give rise to plasma pinching on a time interval much less than the laser cycle without any numerically observable limits within the used QED-PIC treatment.

Although the formation of current structures is a fundamental property of plasma responding to external fields, for the problem of interest intrinsic current interactions play an exceptionally important role because of their high values. It is shown that the pinching effect yields extremely dense pair plasma, and has a strong impact on microscopic characteristics such as particle orbits and γ-ray emission as well as macroscopic plasma parameters. The rapid growth of the plasma-produced azimuthal magnetic field also causes an inductive axial electric field of extreme strength. This may provide a novel pathway for approaching the Schwinger limit

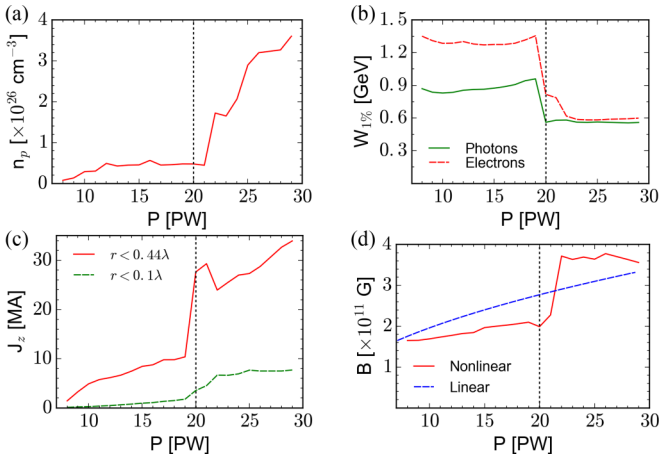

FIG. 1. Plasma-field parameters at nonlinear stage of interaction vs laser power: (a) maximum pair density; (b) maximum photon (solid line) and electron (dashed line) energy; (c) currents through plane $z = 0$ in cylinders $\rho = 0.44\lambda$ (solid line) and $\rho = 0.1\lambda$ (dashed line); (d) maximum magnetic field at linear (dashed line) and nonlinear (solid line) stage of interaction.

despite the accepted view concerning field attainability in vacuum [28,29].

Pair plasma generation. To get an insight into the physics and reduce the laser power threshold for the effect of interest we consider the ideal case of the optimal multibeam configuration of the laser setup in the form of an incoming e-dipole wave, which minimizes the focal volume and maximizes the field strength [30]. The electric field in focus is directed along the z axis. We study the spatiotemporal evolution of laser-produced pair plasma in vacuum by performing 3D simulations with the QED-PIC code PICADOR [31]. The total power P is varied in the range from 15 to 30 PW. The time envelope of the laser radiation is chosen to be close to rectangular with the envelope $E\{B\}(t) = E_0\{B_0\}f(t)$, $f(t) = 0.25[1 - \tanh(-\alpha t)]\{1 - \tanh[\alpha(t - \tau)]\}$, which has rapid fronts and a constant amplitude E_0 (B_0) of electric (magnetic) fields, respectively; here $\alpha = 2.276/T$, the pulse duration $\tau = 5T$, and T is the laser period. The laser wavelength $\lambda = 0.9$ μm is taken according to the XCELS project.

To observe strong effects of cascade plasma a seed target should provide a sufficient number of initial electrons not only for vacuum breakdown but also for creation of e^-e^+ plasma with relativistic critical density during laser impact. As a result of the interaction with a strong prepulse or leading front of laser pulses, a seed target can be destroyed, thus it should be adjusted according to the parameters of laser radiation (contrast, spatial and temporal profiles, peak power). Several techniques to ensure initiation and control of the cascade were presented recently [10,32–34]. Fortunately, the dependence of cascade development time on initial target density is logarithmically weak because in the case of vacuum breakdown plasma density increases exponentially fast and grows by more than an order of magnitude within a laser period at $P > 20$ PW. For the described laser parameters we considered different suitable plasma targets placed into the dipole wave focus: a model spherical micron-size target with a 10^{20}–10^{21} cm^{-3} density and a quite realistic isolated nanorod or nanowire of solid-state density (10^{23}–10^{24} cm^{-3}) with a diameter of tens of nanometers and height up to several micrometers. In cases with an equal number of seed electrons different targets lead to very close results, since spherical targets are compressed and all particles are pushed to the focus (see Supplemental Material [27] for more details).

A cubic grid having size 4 μm $\times$ 4 μm $\times$ 4 μm and number of cells $512 \times 512 \times 512$ is used in simulations. In a dipole wave particles that escape from the focus at a distance more than 2λ have vanishing probability of returning to it, thus the size of the box is sufficient. The time step is chosen to be 0.015 fs. This resolution is sufficient for the process of triggering the pinching effect, while the pinch itself has a singular nature and is thus analyzed using up to 32 times higher resolution for both time and coordinate. At first sight, such excessive 3D modeling may seem unreasonable, because it requires significant computational resources with the finest resolution. Nevertheless, other possible approaches, such as modeling in a 2D cylindrical geometry (r–ϕ coordinates) or using the axial symmetry of the initial problem (r–z coordinates) artificially impose symmetries that may change the dynamics of the pinching problem: symmetry along the z axis eliminates particle escape from the high field region, and the axial symmetry prevents the bending instability development.

We use a perfectly matched layer (PML) [35] as the absorbing boundary condition for the field and the absorbing boundary condition for particles. To set the incoming laser field we use the total field–scattered field technique [36] by setting currents at the closed interface near the PML. For modeling QED cascades an adaptive event generator module [37] is used with separate particle resampling for different particle types. This module uses automatic time step splitting, thus photon emission and decay time are efficiently resolved during the simulations.

We have performed a parametric scan over the laser power to get insight into the nonlinear plasma-field dynamics in case of utmost focusing on the basis of an e-dipole wave. At a laser power exceeding the vacuum breakdown threshold, which is about 7.2 PW, the plasma density starts to grow exponentially in time [10,14]. The intensity in the focus $\sim 10^{25}$ W/cm^2 is much less than the one related to the Schwinger field ($\sim 10^{29}$ W/cm^2), which is needed for the direct pair production. In this case the pair plasma is produced by the QED cascade. The properties of such cascade at the nonlinear stage of cascade development in different field configurations are to a considerable degree yet to be studied. Our simulations indicate that there exists a threshold power $P' = 20$ PW that separates two completely different nonlinear regimes. Previously it has been demonstrated that for laser powers below this threshold, quasistatic regimes with extreme parameters of electron-positron plasma in an e-dipole wave can be achieved even with few-cycle laser pulses. This regime of interaction has been studied in detail in Ref. [14].

However, for $P > P'$ there is a striking feature of the laser-plasma interaction that manifests itself through the rapid and quite unexpected change of maximum magnetic field and plasma properties, such as maximum pair densities, maximum particle energies, and maximum current through the plane $z = 0$ during the interaction, and indicates qualitative

modification of the interaction regime. Taking into account that in the focal region ($\rho \equiv \sqrt{x^2+y^2} < 0.44\lambda$) the electrons and positrons accelerated by the electric field form counterstreaming axial flows, large enhancement of plasma density [see Fig. 1(a)] and axial current especially within a cylinder with a small radius $\rho = 0.1\lambda$ [see Fig. 1(c)] demonstrate not only an increase in the number of pairs, but a significant decrease in the radial size of the plasma structures as well. Moreover, the produced currents are comparable with the Alfven current $17\gamma\beta_z$ [kA] ≈ 20 MA, where $\gamma \approx 1200$ [see Fig. 1(b)] is the Lorentz factor of particles and $\beta_z \simeq 1$ is the axial particle velocity normalized to the light velocity c. Such a strong "wirelike" current in a narrow vicinity of the z axis can generate a magnetic field $2J_z/(\rho c) \approx 10^{11}$ G close to the vacuum field $B_0 \approx 10\sqrt{P}/(\lambda\sqrt{c}) \approx 10^{11}$ G and change particle dynamics, which is signaled by up to 1.4 excess of the magnetic field over B_0 [see Fig. 1(d)] and the drop of the maximum particle energy [see Fig. 1(b)] at $P > P'$. Maximum energy $W_{1\%}$ is defined as the minimum energy of 1% of the most energetic particles. All these observations have led us to the conclusion that a qualitative change of the interaction occurs as a result of the internal plasma mechanism of magnetic field generation which we attribute to the formation of strong axial current. The most appropriate process demonstrating the observed properties is plasma pinching, where the corresponding current-carrying plasma is significantly compressed by the self-generated magnetic field as in the conventional case of static external fields [38]. Unlike the conventional pinch effect, in our case electron-positron plasma interacts with the oscillating laser field.

It should be noted that transition between two regimes occurs in the interval 20–23 PW, thus pinch dynamics can be unstable in this power range. That is why all further considerations are performed for the laser power well above this boundary, namely, for $P = 27$ PW.

Pinching of plasma column. To show qualitatively different dynamics of pair plasmas let us look in detail into the spatiotemporal evolution of electron-positron pair plasma with a focus on highly localized plasma distribution and corresponding field structures in the vicinity of the z axis. In Fig. 2(a) we present the temporal evolution for five-period laser pulse $P = 27$ PW. The spatial distributions of fields, positron and gamma photon densities, are shown in Figs. 2(b)–2(m). During the first two periods, the plasma target is compressed and the exponential growth of electron-positron pair plasma density is established as shown in Figs. 2(b)–2(e). This linear regime was studied in ample detail in Ref. [10]. Charged particles oscillate in the ART regime [6] and emit γ photons predominantly along the z axis. This periodic particle motion together with rapid QED cascade development lead to pronounced density oscillations on the interval $2T$–$5T$ synchronized with the laser wave. At this stage the magnetic field in the vicinity of the axis is low, which is explained by the e-dipole wave magnetic field structure with minimum in the center [see Fig. 2(c)].

The dynamics changes drastically when the current J_z in the cylinder $\rho = 0.1\lambda$ in the center approaches 4–5 MA at $t = 5T$ [see Fig. 2(a)]. Within half of the wave period pair density jumps an order of magnitude and exactly at the same time there appears a huge magnetic field exceeding the unperturbed magnetic field amplitude. The spatial distribution clearly shows the formation of an electron-positron pair plasma column with magnetic field at its boundary [see Figs. 2(f)–2(i)]. This plasma column is compressed by the self-generated magnetic field to a few cells, which leads to a rapid rise in plasma density, and decay through bending instability [see Figs. 2(j)–2(m)]. The process of self-compression is initiated by the laser wave and thus occurs each half of the wave period, which is seen as density and magnetic field peaks on the time interval $5T$–$7T$.

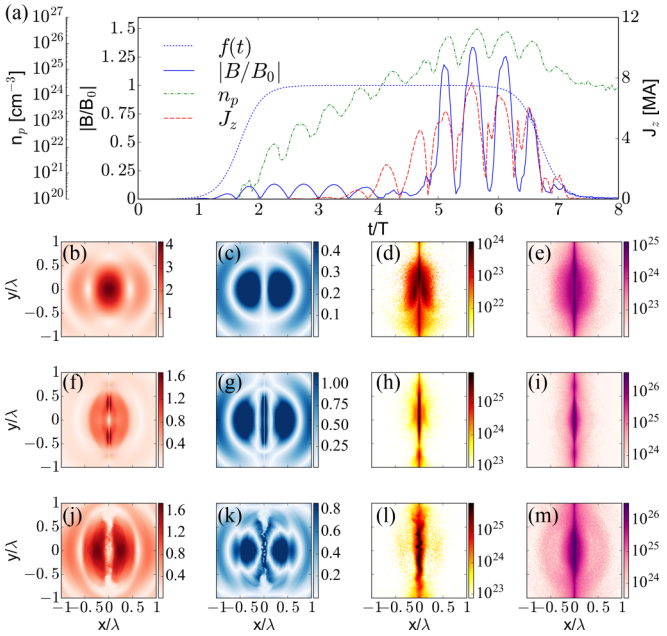

FIG. 2. Plasma-field dynamics for 27 PW. (a) Temporal evolution, $f(t)$: laser pulse envelope; B/B_0: magnetic field in the plane $z = 0$ at $\rho = 1/60\lambda$; n_p: maximum pair density; J_z, current through the cylinder with radius 0.1λ. Electric [(b), (f), (j))] and magnetic [(c), (g), (k)] fields, and positron [(d), (h), (l)] and photon [(e), (i), (m)] distributions at the stages of (b)–(e) linear QED cascade, (f)–(i) plasma column pinching, and (j)–(m) pinch breakdown due to bending instability. For convenience only the central part of the simulation region is shown.

Convergence analysis. To study the effect of limited resolution we have performed a special series of simulations, which show that the pinch dynamics, although being qualitatively similar, quantitatively depends on the simulation resolution.

In Figs. 3(a)–3(f) we present spatial density distributions of the central part of the plasma column and the corresponding magnetic field. The first row corresponds to the initial resolution ($n_\lambda = 115$), and the second and the third rows show the same area with 4 and 16 times higher resolution ($n_\lambda = 460$ and $n_\lambda = 1840$), respectively. The dynamics of the electric and magnetic fields and maximum pair density for different simulation resolutions at the stage of plasma pinching is shown in Figs. 3(g)–3(i). It can be seen that the increase of resolution leads to the monotonic increase of pair-plasma density and fields, resulting in up to seven times increase of magnetic field as compared to vacuum fields and pair density up to 10^{28} cm^{-3} for the highest resolution. To be more

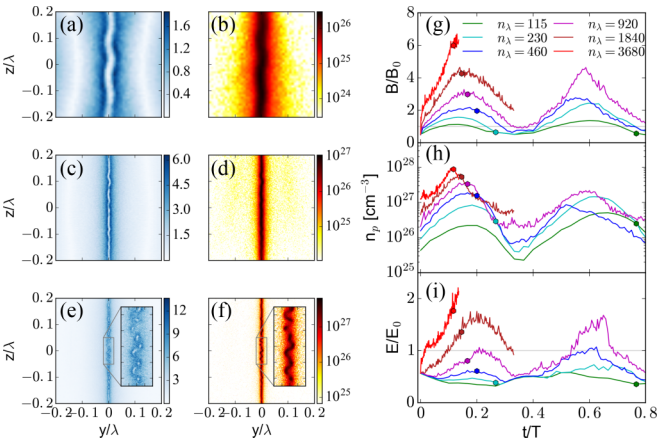

FIG. 3. (a)–(f) Magnetic field [(a), (c), (e)] and pair density distribution [(b), (d), (f)] at the moment of maximum compression and start of bending instability for different resolutions: (a), (b) $n_\lambda = 115$; (c), (d) $n_\lambda = 460$; (e), (f) $n_\lambda = 1840$. (g)–(i) Pinch temporal evolution for different n_λ: (g) magnetic field, (h) pair density, and (i) electric field. Colored dots show the moment of maximum compression and the starting moment of bending instability.

specific we summarized the results of our simulations with different resolutions in Table I. In addition to the magnetic field and pair density, we demonstrate that the electric field may exceed vacuum value. In this case, it is a vortex electric field generated by the changing magnetic field. The power required for obtaining the same level of fields even in the case of optimal e-dipole focusing scales to 132 PW for the electric field and more than 1.2 EW for the magnetic field. We also emphasize that at a quite moderate power of 27 PW the magnetic and electric fields may rise up to 1/20 and 1/40 of the Schwinger field, respectively.

Another important observation is that the time needed to achieve maximum compression, shown as colored dots in Figs. 3(g)–3(i), decreases with the increase of resolution. This observation has led us to the conclusion that self-compression of the plasma column is limited by the simulation resolution and bending instability starts to develop at the moment of maximum compression. If we assumed that the process of compression is limited by bending instability itself, then with the increase of resolution the instability development would

TABLE I. Pinch parameters for different simulation resolutions. n_λ: number of steps per wavelength; n_p: maximum pair density; B/B_0 (E/E_0): maximum magnetic (electric) field normalized to vacuum magnetic (electric) field; P_B (P_E): power of e-dipole wave with the same value of magnetic (electric) field, E_S/B (E_S/E): ratio of Schwinger field to maximum magnetic (electric) field.

n_λ	n_p (cm^{-3})	B/B_0	P_B (PW)	E/E_0	P_E (PW)	E_S/B	E_S/E
115	5.1×10^{26}	1.4	51	0.6	9	100	154
230	1.5×10^{27}	2.4	161	0.7	14	56	122
460	1.9×10^{27}	2.8	207	1.1	31	49	83
920	3.6×10^{27}	3.3	291	1.1	31	42	84
1840	6.5×10^{27}	4.6	583	1.8	83	29	51
3680	9.7×10^{27}	6.7	1212	2.2	132	20	40

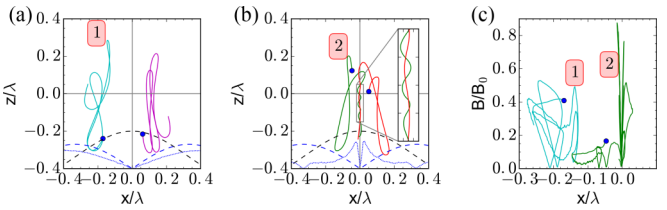

FIG. 4. Typical particle trajectories for (a) 19 PW and (b) 27 PW; (c) phase plane B-x for two trajectories shown in panels (a) and (b). Blue dots show starting points of the trajectories. Dashed lines depict electric (black) and magnetic (blue) fields of an e-dipole wave. Blue dotted line shows self-consistent magnetic field at the nonlinear stage.

be observed at the same moment of time or later. It means that although the pinching process is initiated by the laser wave, since the self-compression rate increases with grid resolution and plasma column is compressed faster, the pinch dynamics is self-consistent in its nature (as opposed to that driven by the external laser field). In fact, this means that the limit of plasma column compression cannot be estimated from simulations, but this series of simulations clearly indicates the pinching nature of the pair plasma dynamics with the formation of extremely dense electron-positron plasma objects and exceptionally high magnetic and electric fields.

A very intriguing question is what the limiting plasma state is, if we do not observe any restrictions within the semiclassical description used in simulations. Here we may assume that they could come from the quantum physics demanding a quantum-mechanical approach to particle motion as well as quantum statistics for plasma description, as was proposed for counterpropagating electron and positron streams in an electron-positron collider [39,40]. This approach may require including other QED processes in existing PIC codes to correctly resolve the dynamics of such plasma.

Particle orbits. It is obvious that the azimuthal magnetic field of high amplitude generated during plasma column pinching should strongly alter single-particle trajectories compared to the case of anomalous radiative trapping (ART) [6], mainly determining particle motion at $P < 20$ PW.

Indeed, the presented typical trajectories for two laser powers of 19 and 27 PW in Figs. 4(a) and 4(b) show this great difference. For the case of 19 PW, ART trajectories corresponding to single-particle motion in the field structure are close to the vacuum standing wave, when plasma does not affect field structure, and all trajectories belong to the half-plane ($x > 0$ or $x < 0$) and do not cross the z axis. The picture is qualitatively different for 27 PW. Now particles are able to oscillate around the z axis due to the large azimuthal magnetic field generated during plasma pinching. To emphasize this fact, we plot in Fig. 4(c) the phase plane B-x, which clearly demonstrates the difference in the motion of these two modes. Since for $P = 19$ PW the particles oscillate between the antinodes of electric and magnetic fields, they experience a half-maximum magnetic field and exhibit complex motion in the B-x phase plane due to stochasticity of photon emission. In the case $P = 27$ PW, the particles first drift to $x = 0$ maintaining the ART pattern of motion in a rising but not too high magnetic field. However, when they reach the axis, the

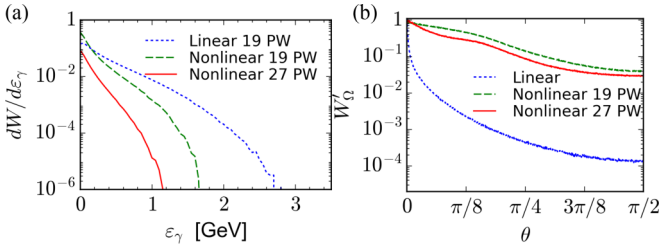

FIG. 5. γ photons: (a) spectra and (b) angular distributions for 19 and 27 PW e-dipole waves.

emerging strong magnetic field ($B \approx B_0$) qualitatively alters their trajectories [41] and in the B-x phase plane the particles show distinctive tracery looking like a set of lengthening loops approaching the axis $x = 0$.

γ-ray emission. As the particles' orbits, energies, and momenta change drastically due to plasma pinching, another important indication of regime modification is alteration of the properties of the emitted photons, such as energy spectra and radiation patterns. First of all, the photon maximum energy changes essentially, which is clearly seen in Fig. 5(a), where the photon spectra averaged over a laser period shrink to 1 GeV, which is consistent with the new type of particle orbits, as the charged particles are now accelerated for a shorter period of time and change the direction of motion more frequently. Second, these features can also be seen in Fig. 5(b), where the radiation pattern is shown in different cases for comparison. In the linear regime, when the particles move predominantly along the z direction, the radiation pattern is extremely narrow with the width of 1 mrad due to the axisymmetric type of radiation, and in the nonlinear regimes the angular pattern becomes more uniform with angular spread up to 0.1 rad relative to the z axis.

In conclusion, we have shown that there are two distinctly different regimes of electron-positron plasma generation by lasers of extreme intensities. The first regime studied recently in Ref. [14] takes place at a power exceeding the threshold of vacuum breakdown via QED cascading but less than about 20 PW. At powers exceeding 20 PW, a new regime of laser-pair plasma interaction is realized, where pinching of the plasma column gives rise to unprecedentedly high pair densities. We show that this effect plays a key role in the laser-pair plasma interactions strongly affecting microscopic characteristics such as particle orbits and γ-ray emission, as well as macroscopic laser-plasma parameters such as pair densities and field magnitudes. It should be emphasized that this interaction regime leading to the generation of very small-scale plasma-field structures is completely different from the conventional mode studied recently [7–9]. In this mode the pinching effect leads to the generation of magnetic and electric fields exceeding the incoming laser fields and thus may provide a novel pathway for approaching the Schwinger field or even for overcoming this limit. Another intriguing consequence of our modeling is that the ultrahigh density quantum pair plasma can be produced by lasers through vacuum breakdown.

Acknowledgments. This work was supported by the Ministry of Education and Science of the Russian Federation under Contract No. 14.W03.31.0032 executed at the Institute of Applied Physics of the Russian Academy of Sciences. The reported research was funded in part (software development and performance optimization) by the Russian Foundation for Basic Research and the Government of the Nizhny Novgorod region of the Russian Federation, Grant No. 18-47-520001. The simulations were performed at the facilities provided by the Joint Supercomputer Center of the Russian Academy of Sciences.

[1] P. Meszaros, Annu. Rev. Astron. Astrophys. **40**, 137 (2002).
[2] G. Sarri, K. Poder, J. M. Cole, W. Schumaker, A. Di Piazza, B. Reville, T. Dzelzainis, D. Doria, L. A. Gizzi, G. Grittani, S. Kar, C. H. Keitel, K. Krushelnick, S. Kuschel, S. P. D. Mangles, Z. Najmudin, N. Shukla, L. O. Silva, D. Symes, A. G. R. Thomas, M. Vargas, J. Vieira, and M. Zepf, Nat. Commun. **6**, 6747 (2015).
[3] A. R. Bell and J. G. Kirk, Phys. Rev. Lett. **101**, 200403 (2008).
[4] S. S. Bulanov, V. D. Mur, N. B. Narozhny, J. Nees, and V. S. Popov, Phys. Rev. Lett. **104**, 220404 (2010).
[5] E. G. Gelfer, A. A. Mironov, A. M. Fedotov, V. F. Bashmakov, E. N. Nerush, I. Y. Kostyukov, and N. B. Narozhny, Phys. Rev. A **92**, 022113 (2015).
[6] A. Gonoskov, A. Bashinov, I. Gonoskov, C. Harvey, A. Ilderton, A. Kim, M. Marklund, G. Mourou, and A. Sergeev, Phys. Rev. Lett. **113**, 014801 (2014).
[7] E. N. Nerush, I. Y. Kostyukov, A. M. Fedotov, N. B. Narozhny, N. V. Elkina, and H. Ruhl, Phys. Rev. Lett. **106**, 035001 (2011).
[8] T. Grismayer, M. Vranic, J. L. Martins, R. A. Fonseca, and L. O. Silva, Phys. Plasmas **23**, 056706 (2016).
[9] M. Jirka, O. Klimo, S. V. Bulanov, T. Z. Esirkepov, E. Gelfer, S. S. Bulanov, S. Weber, and G. Korn, Phys. Rev. E **93**, 023207 (2016).
[10] A. Gonoskov, A. Bashinov, S. Bastrakov, E. Efimenko, A. Ilderton, A. Kim, M. Marklund, I. Meyerov, A. Muraviev, and A. Sergeev, Phys. Rev. X **7**, 041003 (2017).
[11] See http://www.eli-laser.eu.
[12] See http://www.clf.stfc.ac.uk/CLF/Facilities/Vulcan/.
[13] See http://www.lcf.institutoptique.fr/lcf-en/Research-groups/Lasers/Research-Topics/Apollon-10-PW-facility.
[14] E. S. Efimenko, A. V. Bashinov, S. I. Bastrakov, A. A. Gonoskov, A. A. Muraviev, I. B. Meyerov, A. V. Kim, and A. M. Sergeev, Sci. Rep. **8**, 2329 (2018).
[15] A. I. Nikishov and V. I. Ritus, Sov. Phys. JETP **25**, 1135 (1967).
[16] A. Di Piazza, C. Müller, K. Z. Hatsagortsyan, and C. H. Keitel, Rev. Mod. Phys. **84**, 1177 (2012).
[17] L. L. Ji, A. Pukhov, I. Y. Kostyukov, B. F. Shen, and K. Akli, Phys. Rev. Lett. **112**, 145003 (2014).
[18] A. M. Fedotov, N. V. Elkina, E. G. Gelfer, N. B. Narozhny, and H. Ruhl, Phys. Rev. A **90**, 053847 (2014).
[19] J. M. Cole, K. T. Behm, E. Gerstmayr, T. G. Blackburn, J. C. Wood, C. D. Baird, M. J. Duff, C. Harvey, A. Ilderton,

A. S. Joglekar, K. Krushelnick, S. Kuschel, M. Marklund, P. McKenna, C. D. Murphy, K. Poder, C. P. Ridgers, G. M. Samarin, G. Sarri, D. R. Symes, A. G. R. Thomas, J. Warwick, M. Zepf, Z. Najmudin, and S. P. D. Mangles, Phys. Rev. X **8**, 011020 (2018).

[20] K. Poder, M. Tamburini, G. Sarri, A. Di Piazza, S. Kuschel, C. D. Baird, K. Behm, S. Bohlen, J. M. Cole, D. J. Corvan, M. Duff, E. Gerstmayr, C. H. Keitel, K. Krushelnick, S. P. D. Mangles, P. McKenna, C. D. Murphy, Z. Najmudin, C. P. Ridgers, G. M. Samarin, D. R. Symes, A. G. R. Thomas, J. Warwick, and M. Zepf, Phys. Rev. X **8**, 031004 (2018).

[21] T. Wistisen, A. Di Piazza, H. Knudsen, and U. Uggerhøj, Nat. Commun. **9**, 795 (2017).

[22] M. Vranic, T. Grismayer, R. A. Fonseca, and L. O. Silva, Plasma Phys. Controlled Fusion **59**, 014040 (2017).

[23] L. Wen, W.-Y. Liu, T. Yuan, M. Chen, J.-Y. Yu, F. Li, D. Del Sorbo, C. Ridgers, and Z.-M. Sheng, Sci. Rep. **8**, 8400 (2018).

[24] See http://www.xcels.iapras.ru.

[25] J. Kawanaka, K. Tsubakimoto, H. Yoshida, K. Fujioka, Y. Fujimoto, S. Tokita, T. Jitsuno, N. Miyanaga, and G.-E. D. Team, J. Phys.: Conf. Ser. **688**, 012044 (2016).

[26] See http://www.sciencemag.org/news/2018/01/physicists-are-planning-build-lasers-so-powerful-they-could-rip-apart-empty-space.

[27] See Supplemental Material at http://link.aps.org/supplemental/10.1103/PhysRevE.99.031201 for the schematic of interaction and comments on the proposed experimental setup.

[28] S. S. Bulanov, T. Z. Esirkepov, A. G. R. Thomas, J. K. Koga, and S. V. Bulanov, Phys. Rev. Lett. **105**, 220407 (2010).

[29] A. M. Fedotov, N. B. Narozhny, G. Mourou, and G. Korn, Phys. Rev. Lett. **105**, 080402 (2010).

[30] I. Gonoskov, A. Aiello, S. Heugel, and G. Leuchs, Phys. Rev. A **86**, 053836 (2012).

[31] I. Surmin, S. Bastrakov, E. Efimenko, A. Gonoskov, A. Korzhimanov, and I. Meyerov, Comput. Phys. Commun. **202**, 204 (2016).

[32] M. Tamburini, A. Di Piazza, and C. Keitel, Sci. Rep. **7**, 5694 (2017).

[33] I. I. Artemenko and I. Y. Kostyukov, Phys. Rev. A **96**, 032106 (2017).

[34] M. Jirka, O. Klimo, M. Vranic, S. Weber, and G. Korn, Sci. Rep. **7**, 15302 (2017).

[35] J.-P. Berenger, J. Comput. Phys. **114**, 185 (1994).

[36] A. Taflove and S. Hagness, *Computational Electrodynamics: The Finite-Difference Time-Domain Method*, The Artech House Antenna and Propagation Library (Artech House, Inc., Boston, 2005).

[37] A. Gonoskov, S. Bastrakov, E. Efimenko, A. Ilderton, M. Marklund, I. Meyerov, A. Muraviev, A. Sergeev, I. Surmin, and E. Wallin, Phys. Rev. E **92**, 023305 (2015).

[38] G. Benford and D. L. Book, Adv. Plasma Phys. **4**, 125 (1971).

[39] F. Winterberg, Phys. Rev. A **19**, 1356 (1979).

[40] B. E. Meierovich, Phys. Rep. **92**, 83 (1982).

[41] P. Gratreau, Phys. Fluids **21**, 1302 (1978).